Appl. Phys. B 91, 651–660 (2008)
DOI: 10.1007/s00340-008-2971-0

Applied Physics B
Lasers and Optics

A.H. GALMED
M.A. HARITH✉

Temporal follow up of the LTE conditions in aluminum laser induced plasma at different laser energies

National Institute of Laser Enhanced Science (NILES), Cairo University, Giza, Egypt

Received: 22 September 2007 /
Revised version: 31 December 2007
Published online: 13 March 2008 • © Springer-Verlag 2008

ABSTRACT In order to analyze the emission spectrum of a laser-induced plasma for obtaining quantitative information on the abundance of the species present in the plasma it is necessary to study the local thermodynamic equilibrium (LTE) conditions in the plasma and determine the best conditions at which they are satisfied. In the present work Nd:YAG laser light pulses ($\lambda = 1064$ nm, 6 ns) of different energies (25, 50, 75 and 100 mJ) are focused using a quartz lens (focal length 10 cm) onto certified aluminum alloy samples in air under atmospheric pressure. The emitted spectra are collected and analyzed using an echelle spectrometer coupled with an intensified charge coupled device camera. The temporal history of the plasma is obtained by recording the emission features at predetermined delays and at a fixed gate width (2500 ns). For each spectrum both electron density and excitation temperature are calculated for each delay time and laser pulse energy; we found that the values of the electron density are decreasing from 10^{18} to 10^{17} cm^{-3}. The corresponding excitation temperatures were between 30 000 and 4000 K depending on the laser pulse energy and the sample used. The LTE conditions were followed up for the different delays and different energies to determine the temporal range in which they are satisfied. It has been found that in the cases of 25- and 50-mJ laser energies, the LTE conditions were satisfied in the chosen delay range (500–5000 ns). On the other hand, for higher laser energies, the LTE conditions were critical at delay times less than 1500 ns and are satisfied for longer delays.

PACS 52.38.Mf

1 Introduction

The ability of high power pulsed lasers to vaporize, atomize and ionize microquantities of solid samples has resulted in a number of analytical approaches for inspection of solid materials, including depth profiling and multielement imaging based on atomic emission spectrometry [1–3]. One of the most important applications is laser induced breakdown spectroscopy (LIBS).

✉ Fax: +202-35675335, E-mail: mharithm@niles.edu.eg

Laser induced breakdown spectroscopy is an elemental analytical technique based on the non-selective excitation of the atoms constituting the sample, obtained by focusing a pulsed laser beam on its surface. A small amount of target material, of the order of a few microgrammes, is ablated, atomized and ionized producing a plasma plume. After the formation of the plasma, it begins to cool down in a time of the order of a few microseconds. During this cooling down process, the plume emits continuum radiation due to Bremsstrahlung and recombination processes and discrete radiation due to de-excitation processes of atoms and ions present in the plasma [4, 5]. Internal transitions in the excited atoms or ions emit a characteristic spectral pattern, from which the elemental constituents of the sample can be identified. The emitted light spectrum then can be collected, sent to a spectrometer and analyzed to obtain information about the composition of the material under study. Quantitatively, the intensities of the spectral lines are related to the concentrations of the corresponding elements in the plasma plume and consequently in the target material. There are many attractive features for the LIBS technique which make it a valuable analytical tool in a number of different fields, such as the ability to be used with solids, gases and liquids (also non-conducting and conducting materials) and the ability to analyze extremely hard materials that are difficult to digest or dissolve (ceramics and superconductors). Little or no sample preparation reduces the time consumed in the experiment as well as the cost, in addition to the ablation of very small amounts of the material (~ 0.1 to 1 μg), which makes it practically non-destructive. The technique can be used for local analysis in microregions offering a spatial resolving power of ~ 1–100 μm. Also, LIBS furnishes simultaneous multielement analysism which makes it a simple and rapid method of analysis.

In fact, the analytical performance of the LIBS technique depends strongly on the experimental conditions, which have to be carefully examined in each application. These parameters are the laser wavelength [6], the pulse energy [7], the laser pulse duration and shape [8, 9], the time interval of observation and the geometrical set-up of the collecting optics. The choice of the experimental arrangement should be aimed at optimizing the reproducibility of the measurements, while at the same time the conditions for stoichiometric ablation and thin plasma are still fulfilled [10].

In general, to obtain this information by a kinetic description we should solve a complex system of equations describing all the reactions that occur in the plasma accounting for ionization, dissociation, recombination, elastic and inelastic collisions, radiative emission, photon re-absorption and Bremstrahlung processes and all the reactions' rates should be estimated. For that reason the thermodynamical approach is usually preferred, relying on the hypothesis of infinite rate coefficients.

For a thermodynamical description it is essential to keep in consideration the contributions of the different forms of energy present in a laser-induced plasma. The equilibrium distributions of these energies are respectively the Maxwell, Boltzmann and Planck functions, each one characterized by a parameter T (temperature), defined separately and thus a priori different for each different function. It may happen that one or more of these energies is not at equilibrium and does not follow the previous distribution. For instance, this is the case of the radiation emitted from thin plasma, which is not at equilibrium and then does not follow the Planck distribution.

A system is in complete thermodynamical equilibrium (TE) if all the forms of energy are in equilibrium with each other, and this happens when the rate of a reaction is the same as the rate of the inverse process for all processes. In this case the parameter T is the same for all the distributions, assuming the familiar meaning of temperature, and the principle of detailed balance must hold.

Under TE conditions, the population of the excited levels for each species follows the Boltzmann distribution:

$$N_i/N_j = (g_i/g_j)\mathrm{e}^{-(E_i-E_j)/kT}\,, \tag{1}$$

where N_i and N_j are the population densities of the excited levels i and j, respectively. g and E are the statistical weight and the excitation energy of the level, respectively, and T is the temperature.

The population of different ionization stages, in the TE hypothesis, is described by the Saha equation, which in the cases of the neutral and singly ionized species (the only ionization stages present in a typical laser-induced plasma (LIP)) of the same element can be written as

$$N_\mathrm{e}N_\mathrm{i}/N_\mathrm{a} = K_\mathrm{ion}/\alpha_\mathrm{rec} = (2g_\mathrm{i}/g_\mathrm{a})\left(2\pi m k_\mathrm{B}T_\mathrm{exc}/h^3\right)^{3/2} \times \mathrm{e}^{-(E_\mathrm{a}-\Delta E_\mathrm{ion})/k_\mathrm{B}T_\mathrm{exc}}\,, \tag{2}$$

where N_e, N_i and N_a are the plasma electron density and the number densities of the singly ionized species and the neutral atomic species, respectively. K_ion and α_rec are the ionization and recombination rates, respectively. E_a is the energy of the atomic transition while ΔE is the energy of the ionic transition plus the ionization potential of the neutral species in its ground state and m is the electron mass. On the other hand, if the plasma is in full TE, the radiation within it also has a well-defined distribution of energy density which depends only on the temperature. The spectral energy density in vacuum (W) at temperature T, for a single polarization, is given by the Planck function

$$W(\omega) = [h\omega^3/2\pi^2c^3][\mathrm{e}^{h\omega/k_\mathrm{B}T_\mathrm{exc}} - 1]^{-1}\,. \tag{3}$$

In practice, however, this situation cannot be fully realized in a LIP and some approximations must be adopted to describe its state. In LIPs radiative energy is decoupled from the others, since radiative equilibrium requires the plasma to be optically thick at all frequencies (black body). However, typical LIBS plasmas are usually described by a state known as local thermodynamic equilibrium (LTE). This state is reached if the collision processes are much more effective than the radiative processes in establishing the plasma thermodynamics, i.e. if the characteristic collision time $1/\upsilon_\mathrm{col}$ is much less than the characteristic time of radiative decay $\tau_\mathrm{rad} = 1/\Delta\upsilon_\mathrm{nat}$, where $\Delta\upsilon_\mathrm{nat}$ is the natural line width of the plasma emission lines. Under these conditions the non-equilibrium of the radiation can be neglected and the atoms, ions and electrons can be considered at equilibrium. It is thus possible to find a temperature parameter that satisfies both the Boltzmann and Maxwell distributions, and the Saha law. If LTE is a good approximation of the plasma state, the plasma excitation temperature (T_exc) and the electron density (N_e) (which can be easily derived from the emission spectra) can be used to describe the plasma characteristics and the plasma analysis becomes possible.

The inelastic electron collisions with atoms and ions, as described by

$$e + A(m) \rightarrow e + A(n)$$

(where $A(m)$ and $A(n)$ are the atoms or ions in the states m and n, respectively), is the rate-determining mechanism for the transitions of bound electrons from a quantum state to another. The cross section of such a process can be estimated on the basis of the Bethe–Born approximation and takes the form [13]

$$\sigma_{nm} = \left[2\pi e^4 f_{nm}/(\Delta E_{mn})^2\right]\Phi(x)\,, \tag{4}$$

where f_{mn} is the oscillator strength of the considered transition, ΔE_{mn} is its energy jump and $\Phi(x)$ is a dimensionless function of the reduced electron energy $x = \varepsilon/\Delta E_{mn}$ reaching its maximum value $\Phi_\mathrm{max} \approx 0.1$ at $x_\mathrm{max} = 4$.

Since the collisional cross section, as expressed in (4), increases with the quantum number n of the level (decreasing ΔE_{mn}) and the rate of radiative decay A_{mn} reduces with n, it is clear that the LTE condition holds more easily for high quantum levels. If there is a level n' for which the collision and radiative rates are the same, then we are in partial LTE (pLTE) conditions, where the level $n > n'$. The condition that the collision rate is much higher than the radiative rate can be expressed by $\langle\sigma_{mn}\upsilon\rangle \gg A_{mn}$, which is a condition on the electron density, which in turn is the parameter determining the validity or failure of the LTE.

For hydrogen-like atoms, Griem [11] found a similar condition on electron density (expressed in cm^{-3}) for which a level n is in pLTE (with a confidence of 10% because τ_rad is in any case finite) [11]:

$$N_\mathrm{e} \geq 7\times10^{18}(z^7/n^{17/2})\left(k_\mathrm{B}T_\mathrm{exc}/z^2E_\mathrm{H}\right)^{1/2}\,. \tag{5}$$

So, in a hydrogen plasma the population of the third level is (with a confidence of 10%) in LTE with higher levels if $N_\mathrm{e} \geq 1.7\times10^{14}\,\mathrm{cm}^{-3}$. More generally, the corresponding

lower limit of electron density N_e is given (in cm^{-3}) by the McWhirter criterion [12, 17, 18, 32]

$$N_e \geq 1.6 \times 10^{12} T_{exc}^{1/2} \Delta E^3 , \quad (6)$$

where ΔE (eV) is the highest energy transition for which the condition holds, and T_{exc} is the plasma temperature. This criterion is a necessary, though insufficient, condition for LTE. According to this criterion, for the lower levels to be in LTE, electron densities are required of the order of 10^{19}–10^{20} cm^{-3}, a value hardly reachable in a typical LIP but reachable in air or at high pressure of ambient gas; at lower electron densities in fact the effect of radiative decay becomes important and the levels with low quantum numbers, e.g. the ground level, tend to be overpopulated with respect to the LTE predictions. Fortunately, for these levels, the self absorption of radiation is often important; this effect tends to lower the population and to re-equilibrate it towards the LTE values. Considering the self absorption, the thresholds derived by Griem and McWhirter become lower and reachable in LIBS experiments.

In a time-evolving plasma, besides the above-mentioned McWhirter criterion, expressed in (6), a further condition must hold to have LTE. Since the plasma expands and cools, it is necessary that the characteristic time on which T_{exc} and N_e change ($\Delta T_{exc}/T_{exc} \approx \Delta N_e/N_e \approx 1$) is much longer than the time τ_{rel} needed to cause the plasma to equilibrate (which corresponds more or less to the collision time, if (6) holds). In this case the plasma evolves passing through a succession of LTE states. If this is not the case, the plasma evolves too fast and does not reach equilibrium. This condition is more easily fulfilled at later times of evolution than at early times, where the plasma has slowed down its evolution, and at atmospheric pressures rather than in vacuum experiments since N_e is higher and the expansion is slower.

Finally, the inhomogeneity of the plasma must also be taken in account to establish if the LTE condition is fulfilled or not. It is in fact necessary that the typical length of variation of the parameters T_{exc} and N_e is much higher than $L_{dif} = (D\,\tau_{rel})^{1/2}$, the diffusion distance traveled by a particle during the time of relaxation to equilibrium, τ_{rel}, i.e.

$$[T_{exc}\,(x=0) - T_{exc}(x=L_{dif})]/T_{exc}\,(x=0) \ll 1 ,$$
$$[N_e\,(x=0) - N_e\,(x=L_{dif})]/N_e\,(x=0) \ll 1 . \quad (7)$$

If these conditions are not verified the states of excitation and ionization in each point are not determined by the temperature in that point but by the 'history' of the particles, i.e. by some averaged value on distances of the order of L_{dif}. This condition is more easily violated in the external layers of the plasma where T_{exc} and N_e are lower (and then τ_{rel} and L_{dif} are higher). The problem of the existence of thermodynamic equilibrium in laser-induced plasmas has been investigated by many researchers with both an experimental and a theoretical approach. In some cases, after building an appropriate model of plasma evolution, computer simulation has been used extensively to predict the physical characteristics of the plasma, especially the patterns of electron density and temperature. It is worth mentioning, for instance, the works of Capitelli et al. [13] and De Giacomo et al. [14] that described the evolution of a laser-induced TiO plume at low pressures and of Colonna et al. [15] that discussed more generally the LTE problem in typical LIPs. A number of experimental characterizations of laser-induced plasmas in terms of the T_{exc} and N_e values have also been reported: typically, at a laser fluence of the order of a few J/cm^2, T_{exc} ranges from a fraction of an eV to a few eV, and N_e ranges from 10^{16} to 10^{19} cm^{-3}.

From an experimental perspective, the occurrence of LTE in LIBS plasmas has been assessed by comparing either the actual population of atomic and ionic levels with the theoretical Boltzmann distribution [16] or the temperature values derived from the excited-level populations (excitation temperature) with that derived from the ionization-stage populations by the Saha equation (ionization temperature) [17–20] or derived from the vibrational transitions of molecules (vibrational temperature) [21]. All the works seem to agree in the conclusion that LTE is fulfilled in typical LIPs except in the early time of evolution (1–2 μs) [22]. De Giacomo et al. [14], though this work studied the evolution of a TiO LIP at low pressures and the typical times for the onset of LTE conditions (100–300 ns) are generally lower than the typical times observed at atmospheric pressure. This may be confirmed by a calculation of the typical characteristic times for a plasma [15]. For a laser plasma at an early stage of its evolution $\left(N_{atom} \approx 3 \times 10^{19}\ cm^{-3},\ T_{exc} \approx 2\text{–}10\ eV\right)$ the relaxation time is in the range of $\approx 10^{-6}$–10^{-5} s and the characteristic expansion time, $\approx d/v$, where d are the plasma dimensions and v its expansion velocity, is in the same range of values. The same calculation for lower temperatures ($\approx$ 0.6–0.9 eV) brings a more favorable situation. However, even if we consider the plasma after 1–2 μs where the LTE condition, as observed, is generally fulfilled, it is clear that the reliability of this hypothesis depends heavily on parameters such as the laser energy, pulse duration, ambient gas, acquisition gate, etc., that are used in the actual experiment. It is therefore advisable to carefully choose these parameters as accurately as possible, checking the validity of the LTE approximation a posteriori in order to find the optimized experimental setup.

In the following work, we will study the LTE conditions temporally at different laser energies for different samples to see experimentally the effect of different laser energies and different aluminum matrices on these conditions and to determine experimentally the suitable conditions for LIBS measurements.

2 Experimental procedures

For the experimental part of this work, the plasma was produced by focusing the fundamental wavelength (1064 nm) of the Nd:YAG laser (25, 50, 75 and 100 mJ, 6 ns) onto the surface of certified samples (S1, S2 and S3) (Table 1) in air at atmospheric pressure via a quartz lens of 10 cm focal length. In the focus the laser light fluence corresponding to each of the incident laser energies is 11.8×10^6, 23.6×10^6, 35.4×10^6 and 47.2×10^6 J/m^2, respectively. The plasma emission was collected using a quartz optical fiber with an aperture of 600-μm diameter. The aperture of the optical fiber was aligned with the center line of the plume to keep the emission-signal collection perpendicular with respect to the plasma plume symmetry axes. The fiber–plasma plume distance was adjusted to ensure that the acceptance

Sample number	Code	Al	Cu Be	Fe Ca	Mg Cd	Mn Co	Ni Ga	Si Li	Ti Na	Zn Sr	Bi V	Cr Zr	Pb Sb	Sn P
S1	5182 AP	94.30238	0.061	0.27	4.67	0.35	0.015	0.11	0.053	0.045	0.016	0.015	0.024	0.011
	(10293)		0.0009	0.0025	0.0011		0.015	0.0025	0.00211	0.00231	0.025	0.0037	0.0015	0.001
S2	7010 AA	88.4351	1.88	0.22	2.44	0.082	0.058	0.11	0.061	6.41	0.017	0.041	0.021	0.023
	(10304)		0.0001	0.0036			0.02	0.0042	0.0059	0.0031	0.021	0.14		0.004
S3	356.2 AH	91.7407	0.081	0.16	0.42	0.034	0.033	7.2	0.11	0.075	0.02	0.023	0.017	0.015
	(10342)		0.0013	0.0032			0.021	0.0017	0.0021	0.012	0.022	0.0033	0.0027	0.002

TABLE 1 Sample compositions

solid angle of the fiber covers most of the plume emission to avoid any inhomogeneity in the LIP. The output of the optical fiber was connected to the echelle spectrometer coupled to an intensified charge coupled device (ICCD) camera, allowing simultaneous spectral analysis in the range of 200–900 nm with a constant spectral resolution $\lambda/\Delta\lambda = 7500$.

A gate width of 2500 ns was chosen for maximizing spectral line intensity while maintaining a good temporal resolution. The gate width and delay time for the spectroscopic data acquisition were controlled by computer. To optimize the signal-to-noise ratio and spectral reproducibility, the acquisition of the spectra was carried out by averaging 10 single accumulated spectra preceded by two single shots for cleaning the sample surface. To avoid any inhomogeneity in the sample, the average spectra at five different positions on the sample are taken in each measurement. To avoid the angular dispersion of LIP, measurements were performed at distances from the target surface shorter than or comparable to the spot dimension. The analysis of the emission spectra was accomplished using the commercial 2D/ and 3D/GRAMS/32 software. The laser energy was measured by a Scientech power meter (model AC5001, USA) and then monitored using a fast photodiode and an oscilloscope. The experimental setup is described in detail elsewhere [23].

The plasma emission spectrum was recorded at several delay times (from 0 to 10 000 ns) while varying the pulse energy (25, 50, 75 and 100 mJ) at atmospheric pressure using attenuators to avoid variations in the beam profile by varying the flash-lamp voltage. Temporally resolved optical emission spectroscopy is used to investigate the evolution of the spectral line intensity and broadening, and to estimate temperature and electron density as a function of delay time and pulse energy (calculations are done only in the region of 500 to 5000 ns). The line broadening was calculated by LIBS^{++24} software using Voigt fitting. The width of the spectral lines was measured using the emission line of a He:Ne laser.

3 Results and discussion

3.1 *Plasma properties*

3.1.1 The intensity profile. The emission spectra of the aluminum LIP have been observed at different delay times (0–10 000 ns), constant gate width (2500 ns) and different laser energies (25, 50, 75 and 100 mJ) for the certified samples S1, S2 and S3. Typical emission spectra at two delay times and 100-mJ laser pulse energy are shown in Fig. 1.

The temporal behavior of the LIP of the different samples is generally the same. By the analysis of the spectrum, we can see that at the early stages of plasma evolution (at short delay times) the continuum emission is high, due to mechanisms involving free electrons (inverse Bremsstrahlung, radiative recombination and photoionization) (Fig. 1).

So, we cannot obtain accurate information about atoms and ions because of the overwhelming continuum emission for short delay times (some tens of nanoseconds after the end of the laser pulse). At these early times, the electron density is

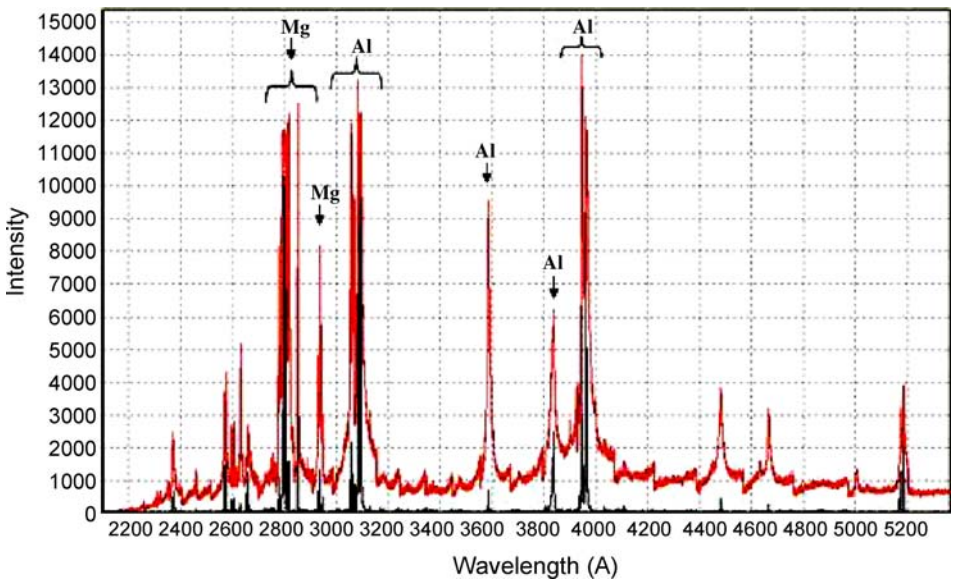

FIGURE 1 Typical spectra at laser energy 100 mJ, gate width 2500 ns and delay time (100 ns in *red* and 2000 ns in *black*)

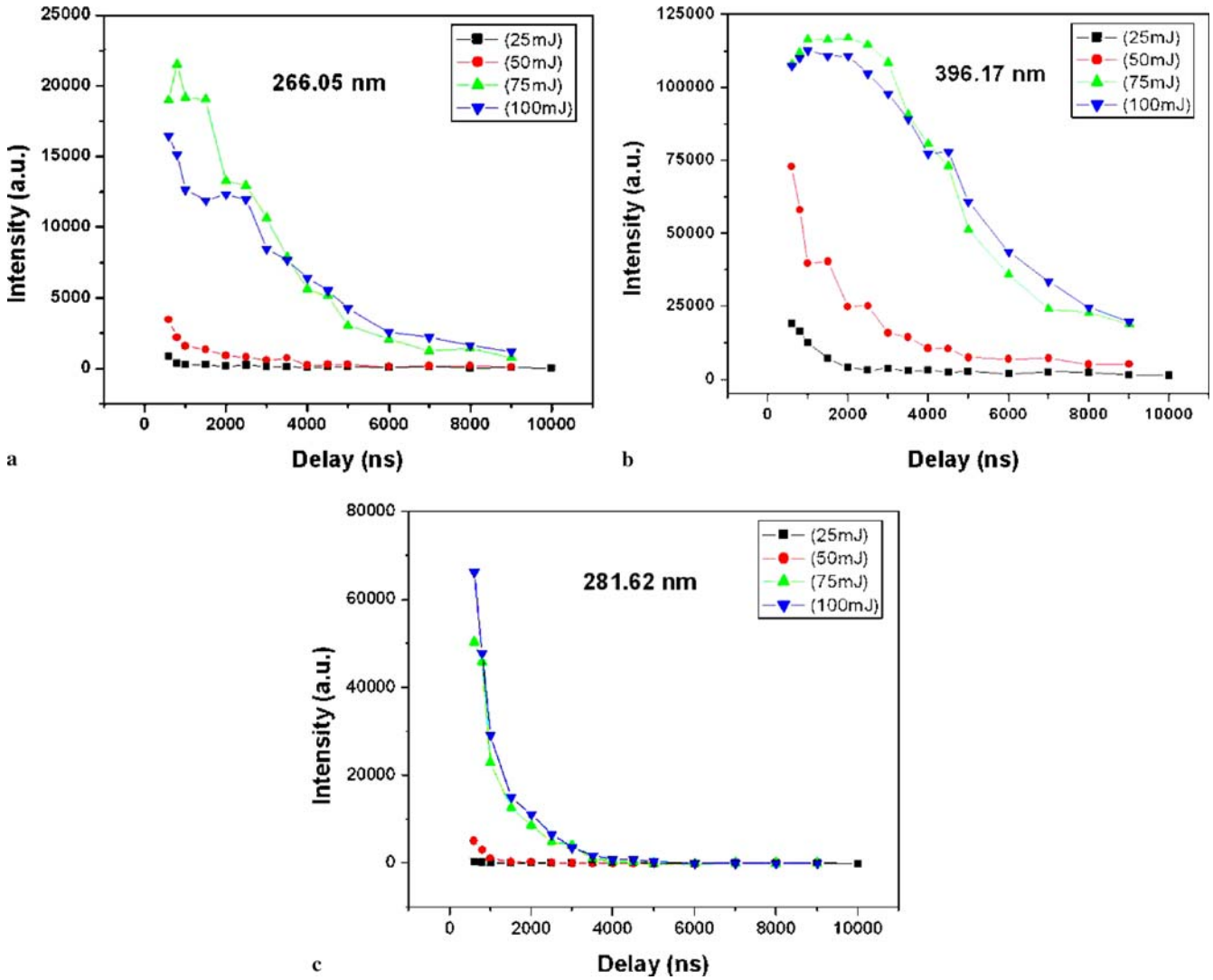

FIGURE 2 The intensity as a function of delay time at different laser energies for the aluminum lines: (**a**) 266.05 nm, (**b**) 396.17 nm and (**c**) 281.62 nm

still very high and the Al I and Al II lines are broadened by the Stark effect due to the electron collisions. At later times of the plasma expansion, the spectral lines become smaller and narrower, indicating a decrease of the electron density (as will be seen later). It is evident that for higher laser energy the continuum is higher and lasts for longer times [25]. As mentioned before in the experimental part, each spectrum is the average of five spectra at five different positions on the sample. Little differences were observed between the five collected spectra, so an error of 15% for typical LIBS experiments is considered in the calculations (especially for the excitation temperature (T_{exc}), the ion temperature (T_{ion}) and the electron density (N_e)). Table 2 lists the spectral parameters of the emission lines used.

In order to study the behavior of the spectral line intensities throughout the experiment, a relation between the line intensity and the delay time for the three chosen lines at different laser energies is drawn in Fig. 2.

Figure 2a represents this relation for the atomic line at 266.05 nm in the sample S1 for different laser energies. Again, the increase of the intensity with higher incident laser energy is clear. At 25 mJ it has been found that the intensity

Line (nm)		E_m (cm^{-1})	E_n (cm^{-1})	A_{mn} (10^8 s^{-1})	g_m
Al II	281.62	143 647	108 159	3.83	1
Al I	256.84	38 929	0.0	0.22	4
Al I	266.09	37 689	0.0	0.264	2
Al I	309.3	32 435	29 067	0.12	4
Al I	394.43	25 348	112	0.493	2
Al I	396.18	25 348	0.0	0.98	2
Mg II	279.55	97 432	61 701	2.6	4
Mg I	285.21	35 085	0.0	4.95	3

TABLE 2 Spectral line characteristics

is low and decreases slightly at early delay and levels off after about 1500 ns. The same behavior is pronounced for the 50-mJ curve at somewhat higher intensity.

A quasi-exponential decay of the spectral line intensities with the delay time is recorded in the cases of 75- and 100-mJ laser pulse energies. Small differences are observed between the results obtained at such two higher incident energies. This may be, as mentioned before, a result of self absorption, which is more probable in the colder plasma regions.

Figure 2b depicts the same relation but for the atomic resonant aluminum line at 396.17 nm. The general behavior is the

same as Fig. 2a but, at higher energies, the self absorption is much more pronounced, leading to the appearance of a broad peak extending to about 4000 ns.

The aluminum ionic line intensity at 281.62 nm is plotted versus the delay time in Fig. 2c. In this case, the behavior of the line is slightly different, since the ionic lines appear in the early stage of the plasma lifetime and decay faster than the atomic lines due to the recombination processes of electrons and ions [26], so we can observe that there is no difference in the intensity of such a line at the different laser energies for delay times > 3500 ns. The same behavior was observed on studying the other two samples S2 and S3. Also, we can observe the proportionality between the line intensity and the laser energy. This is due to the fact that the ablated mass per pulse and the temperature increase with the laser energy [27].

On changing the sample the only change that took place is that at the energies of 25 mJ and 50 mJ the maximum intensity is always observed at higher energy, while the intensity of the lines at 100 mJ is found to be nearly equal to that of the spectra obtained at 75 mJ. This is also a result of the self absorption that shows up more strongly at higher laser pulse energies due to the existence of more ablated mass.

3.1.2 Electron density. The electron density can be estimated from studying the Stark broadening of a well-isolated line in the plasma emission, since the other broadening mechanisms (Doppler effect, Van der Waals broadening and resonance broadening) can be neglected [28]. In the present case the Al II line at 281.62 nm was used. The FWHM of a Stark-broadened line $\Delta\lambda_{1/2}$ is related to the electron density N_e (cm^{-3}) by the following expression [29]:

$$\Delta\lambda_{1/2}(\text{Å}) = 2w\left(N_e/10^{16}\right) + 3.5A\left(N_e/10^{16}\right)^{1/4} \times \left[1 - BN_D^{-1/3}\right] w\left(N_e/10^{16}\right) , \quad (8)$$

where w, A and N_D are the electron impact parameter, the ion broadening parameter and the number of particles in the Debye sphere, respectively. B is a coefficient equal to 1.2 and 3/4 for ionic and neutral lines, respectively. The values of A and w were taken from Griem [11] and Colon et al. [28] for Al lines, at an appropriate temperature. The contribution from the quasi-static ion broadening second term in (8) is negligible. Therefore, assuming that $A = 0$, (8) leads to

$$\Delta\lambda_{1/2} = 2wN_e/10^{16} . \quad (9)$$

The chosen spectral line was fitted using Voigt fitting and the Lorentzian width (w_l) of the line has been taken as $\Delta\lambda_{1/2}$, while the Gaussian width (w_g) is the instrumental line broadening that is predetermined using the line width of the He:Ne laser line, $w_g = 0.6$ Å. The line broadening w_l has been calculated using the equation

$$\Delta\lambda_{1/2} = \left[\left(w_g^2 + (w_l/2)^2\right)\right]^{1/2} + w_l/2 .$$

In this way, it was possible to eliminate the instrumental broadening (Fig. 3). $\Delta\lambda_{1/2}$ is the full width at half maximum ($FWHM_{exp}$) of the experimental spectral line. The Voigt fitting of the Al ionic line at 281.62 nm eliminates the asymmetric broadening in this line, which is due to the static Stark ion effect [30, 31].

The electron density (N_e) as a function of the delay time in all the samples was found to have the same behavior, where N_e decreases exponentially with the delay time. The values of the electron density N_e differ slightly from one sample to another but within the same order of magnitude and within the range of the experimental errors. The value of the electron density was found to be decreasing in the range of 6.1×10^{18} cm^{-3} to 6.7×10^{17} cm^{-3} in the delay range (100 ns to 3000 ns). These values were similar to those obtained by Barthélemy et al. [32]. There were no appreciable changes in the values of the electron density N_e at different laser energies. Since N_e is calculated from the line (Al II at 281.62 nm), its value may be affected by the self absorption in the case of high laser pulse energies. However, this effect on the N_e values is not clear within the range of the experimental error, as can be

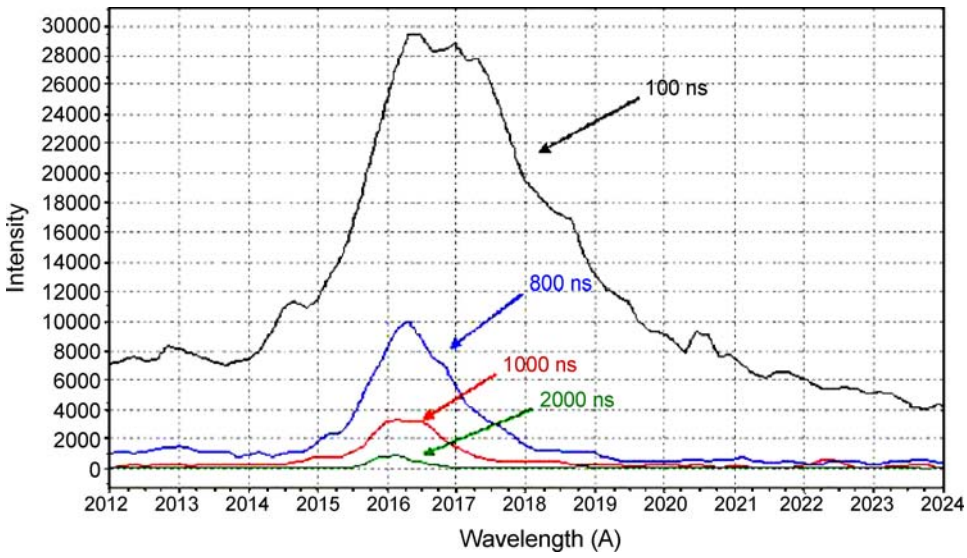

FIGURE 3 The line broadening of the Al II line at 281.68 nm at 50-mJ laser energy for different delay times

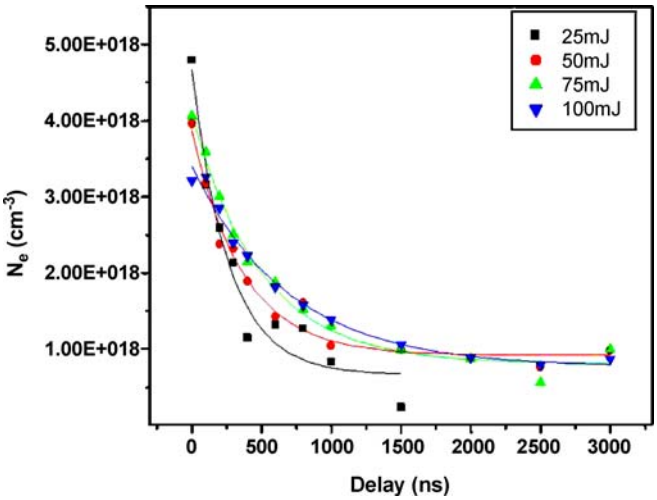

FIGURE 4 The electron density (N_e) as a function of delay time at different laser energies for the sample S2

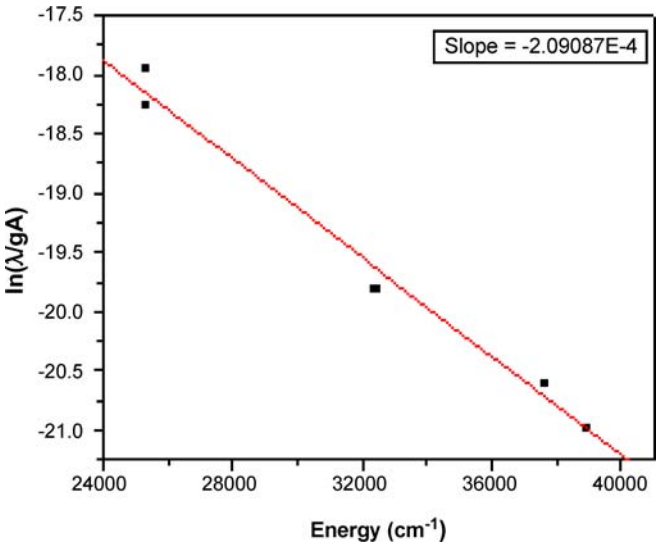

FIGURE 5 Boltzmann plot at laser pulse energy 50 mJ and delay time 1000 ns

seen from Fig. 4. There is no noticeable difference in the electron densities between the samples in Fig. 4. However, some differences may arise due to using targets differing in their percentage elemental compositions, i.e. representing different matrices [33].

3.1.3 Excitation temperature. The excitation temperature (T_{exc}) is determined via the well-known Boltzmann plot method from the relative line intensities, provided that their transition probabilities (A_{mn}) from a given excitation state are known. This method implies the assumption of LTE but, taking into consideration the high electron density in our plasmas, this assumption seems to be satisfied at least during the first 5 μs of the plasma lifetime. Therefore, the populations of the excited states follow a Boltzmann distribution, and their relative emissivities (I_{mn}) can be given by [17, 18, 32, 34, 35]

$$\ln(\lambda_{mn} I_{mn}/g_m A_{mn}) = \ln(N(T)/U(T)) - E_m/k_B T_{exc}\,, \qquad (10)$$

where λ_{mn} and A_{mn} are the wavelength and the transition probability of the transition between the two levels m and n, respectively. g_m and E_m are the statistical weight and the energy of the excited level m. k_B is the Boltzmann constant, $U(T)$ is the partition function and $N(T)$ is the atomic or ion density. Then, on drawing the Boltzmann plot (Fig. 5), the excitation temperature can be estimated by the relation $S = -1/(kT_{exc})$, where S is the slope.

The excitation temperature T_{exc} was estimated from the emission intensity of five aluminum (Al I) lines in the laser-induced plasma of one of the aluminum alloys. Table 2 lists some spectral lines and their constants. The wavelengths, statistical weights and transition probabilities of these lines are found in Griem [11], Colon et al. [28] and Barthélemy et al. [32].

As was mentioned before, the study was performed on three certified aluminum samples at four different laser energies. In the case of the sample S1 it was found that the value of the excitation temperature T_{exc} increases as the laser energy increases. From 100-ns to 3000-ns delay times, the corresponding values for T_{exc} ranged from 30 000 K in the case of 100 mJ to 5500 K in the case of 25 mJ. The same behavior was observed for the other two samples (S2 and S3) but with different T_{exc} values (Fig. 6a). The T_{exc} decay follows the first-order exponential decay fitting done by the original program.

Two main behaviors were observed in the previous results. First, as the laser energy increases T_{exc} increases and this is expected because the kinetic energy gained by the electrons increases as the deposited laser energy increases. Second, as the laser energy increases T_{exc} decays faster. This fast T_{exc} decay is due to the large difference between T_{exc} and the ambient temperature, which allows the energy transfer to be faster. In addition, the high value of T_{exc} makes the plasma expand faster and consequently the rate of cooling of the plasma is faster. Also, it was observed that there is no dramatic change in T_{exc} for the different samples, especially for lower laser energies (25 mJ and 50 mJ), which reflects the negligible matrix effect.

3.1.4 Ionization temperature. The ionization temperature (T_{ion}) was calculated using the Saha–Boltzmann equation [17, 32] (which is derived from the Saha law [32]) using the two magnesium lines (Mg I 285.21 nm) and (Mg II 279.55 nm) (Table 2):

$$I_{ion}/I_{atom} = \left(4.83 \times 10^{15}/N_e\right)(gA/\lambda)_{ion}(\lambda/gA)_{atom} T_{ion}^{3/2} \times \exp(-(E_{ion} - E_{atom})/k_B T_{ion})\,, \qquad (11)$$

where I_{ion} and I_{atom} are the ionic and atomic line intensities, respectively, g is the statistical weight and A is the spontaneous transition probability. The values of E_{ion} and E_{atom} were obtained from Barthélemy et al. [32] (Table 1). T_{ion} was found to have nearly the same behavior for all cases but with different values, as is clear from Fig. 6b.

Since the ionic line (Mg II 279.55 nm) is very near to other Mg lines, at the higher laser energy, especially for early delay times, those lines interfere with each other giving rise to error in calculating T_{ion}. So, we used the calibration free software LIPS^{++}[24] in order to make a Voigt fitting for those lines and separated them to obtain the real line intensity for each. For

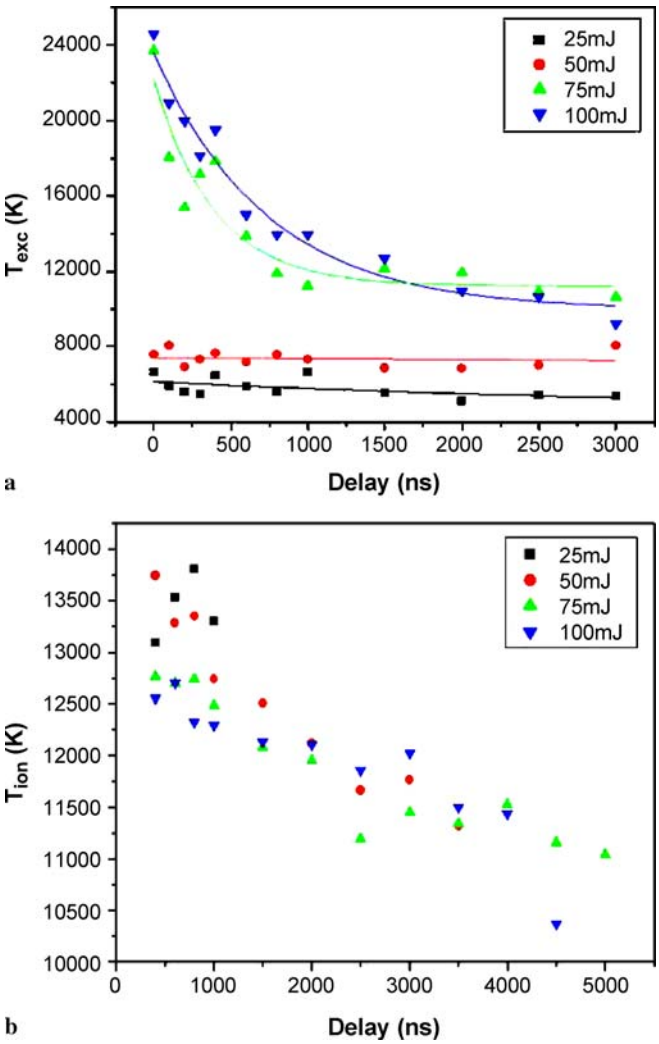

FIGURE 6 (**a**) The excitation temperature (T_{exc}) and (**b**) the ion temperature (T_{ion}) as a function of delay time at different laser energies for the sample S2

all samples the general behavior of the ionic temperature is the same with variation of the laser energy within the range of the experimental error in the delay time interval (500 ns to 5000 ns). As expected, the decrease of the ionization temperature T_{ion} throughout the mentioned delay range is relatively slow. In the cases of samples S1 and S2, T_{ion} was found to decrease from 13 500 to 10 000 K, while for sample S3 the ionization temperature decreases from 14500 to 10 000 K.

3.2 *LTE conditions*

The Boltzmann equation, the Maxwell equation and the Saha equation that are used to calculate the laser induced plasma parameters (T_{exc}, T_{ion}, N_e, ..., etc.) rest on the essential assumption that such transient plasma is in local thermal equilibrium (LTE). So, if the plasma is out of the LTE conditions the previously mentioned equations will not be valid, leading to a vast deviation in the spectrochemical analysis in the LIBS experiment [31].

For the plasma to be in LTE, atomic and ionic states should be populated and depopulated predominantly by collisions rather than by radiation. This requires that the electron density has to be high enough to ensure a high collision rate. The corresponding lower limit of electron density is given by the McWhirter criterion [36]

$$N_e \geq 1.6 \times 10^{12} T_e^{1/2} \Delta E^3 , \tag{12}$$

where ΔE (eV) is the largest energy transition for which the condition holds ($\Delta E = 4.5$ eV) [17] and T_e (K) the plasma temperature.

In general in all cases the McWhirter criterion was found to be fulfilled and is not affected by changing the laser energy or sample. In the case of 25-mJ laser energy, we were not able to investigate the McWhirter criterion after 1500-ns delay time because of the disappearance of the ionic line at 281.62 nm by which we calculate the electron density N_e. Since the McWhirter criterion is necessary but not sufficient for confirming the LTE conditions, we had to confirm our results. This was done by comparing T_{exc} and T_{ion} for each laser energy in each sample (Fig. 7). Although T_{exc} is calculated from Al lines and T_{ion} is calculated from Mg lines, they can be compared since there are no differences between T_{exc} values calculated from any element in the same sample if the LTE conditions are satisfied [17].

In the cases of 25- and 50-mJ laser energies, the values of T_{ion} are much higher than those of T_{exc} in all samples, indicating that the LTE conditions are not fulfilled in the studied delay time range. At the laser energies of 75 and 100 mJ, the samples S1 and S2 show an increase in T_{exc} relative to T_{ion}, but in fact the differences in T_{exc} and T_{ion} values are still within the range of the experimental error (15%). This indicates that the LTE conditions are fulfilled in the studied delay time range. However, in the case of 75-mJ laser pulse energy it seems that the difference is going in the direction of violating the LTE conditions for longer delay times. In the case of sample S3, although T_{ion} looks higher than T_{exc}, the differences are still within the experimental error range indicating that the LTE conditions are satisfied in the whole delay range.

Milan and Laserna [18] measured the temporal evolution of excitation temperature, calculated by the Boltzmann plot, and ionization temperature, calculated by the Saha equation, in a laser-induced silicon plasma during the first 2 μs of the plasma lifetime. The authors found a systematically lower value for the excitation temperature, but with the two values approaching each other with time and reaching a similar value after 2 μs. This result makes us think that at early times the plasma evolves too fast bringing rapidly the N_e values too low for achieving the LTE condition. So, the electron–atom and electron–ion collision rates become comparable with the radiative decay rate, leading to non-LTE plasma where the Saha equation is not fulfilled. We can thus say that the fast evolution does not allow the plasma to pass through equilibrium states. After 1–2 μs, the evolution is considerably slower, and the plasma can reach the equilibrium.

Milan and Laserna's results were a little different to those we observed. This may be due to the difference between the wavelengths used in both works or because Milan and Laserna used silicon plasma and not aluminum plasma.

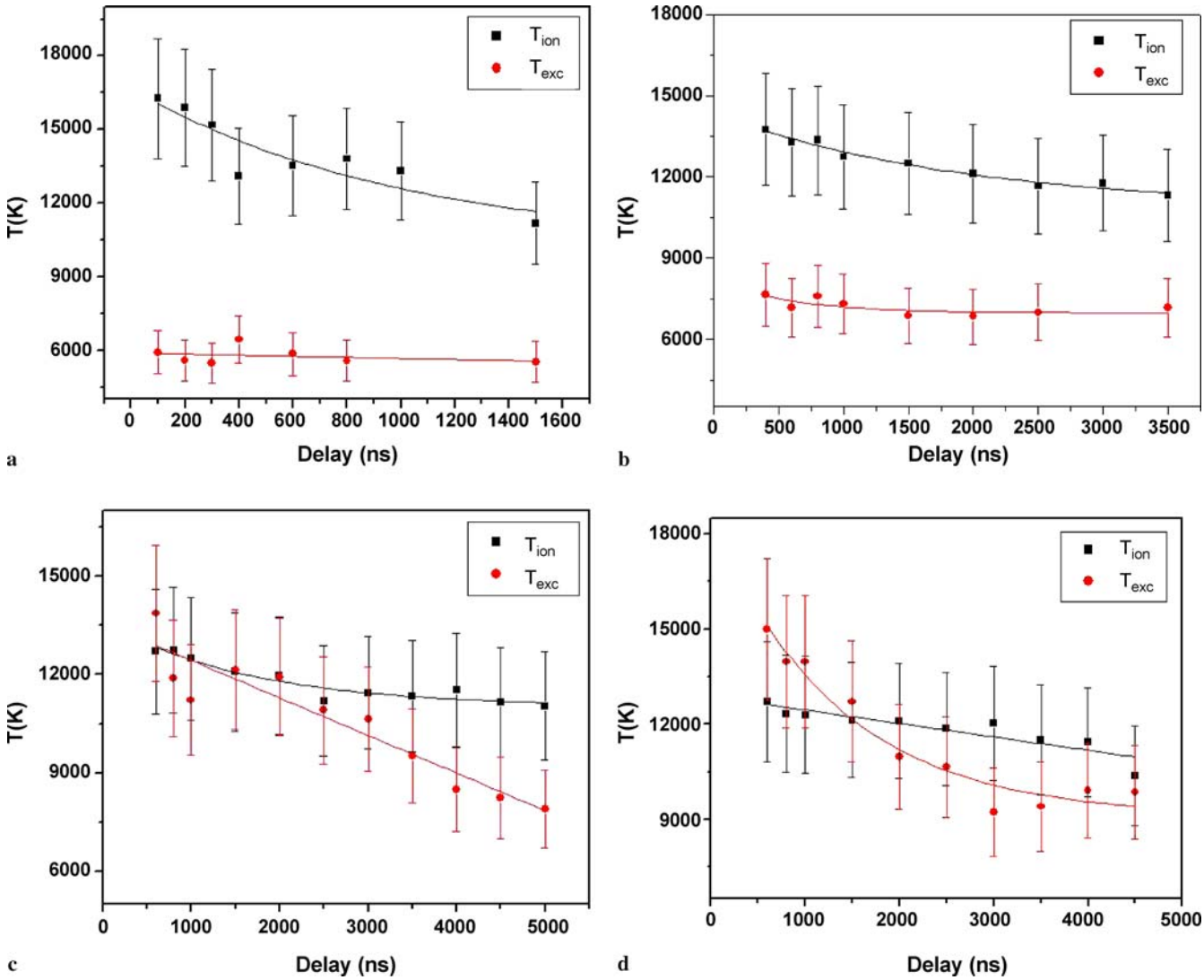

FIGURE 7 Comparison between the ion temperature (T_{ion}) and the excitation temperature (T_{exc}) as a function of delay time at different laser energies for the sample S2: (**a**) at 25 mJ, (**b**) at 50 mJ, (**c**) at 75 mJ and (**d**) at 100 mJ

4 Conclusion

In summary, we have demonstrated that the emission line intensities increase on increasing the laser pulse energy until they level off due to self absorption. At each of the laser pulse energies used (25, 50, 75 and 100 mJ) the line intensities decrease exponentially as the delay time increases due to plasma expansion. The matrix effect appears only in the intensity profile in the case of 50-mJ laser pulse energy. Nearly the same values have been obtained for the electron density (N_e) at different laser energies and for different samples. Boltzmann plots revealed values for the excitation temperatures (T_{exc}) that increase on increasing the laser pulse energy to stabilize at higher laser energy due to spectral line self absorption in the plasma plume.

Following the LTE conditions, we found that the McWhirter criteria are fulfilled for all laser energies and all samples. But, since it is a necessary but not sufficient condition, we compared the T_{exc} and T_{ion} values to confirm our results. From this comparison it has been found that in the cases of laser pulse energies of 25 and 50 mJ the LTE conditions are not fulfilled along the delay time interval under study (500 to 5000 ns). However, in the cases of 75- and 100-mJ laser pulse energies, the LTE conditions are fulfilled in the whole studied delay time range. This may be as a result of the effect of the initial plasma conditions that depend on the incident laser pulse energy [37]. Deviation from LTE for lower laser fluences is due to the less dense plasma, in particular the lower electron density.

In general, it has been demonstrated that the laser pulse energy is an important parameter that affects laser induced plasma parameters, especially its emissivity and temperature, which in turn affect the LTE conditions in the plasma plume.

REFERENCES

1 D. Anglos, S. Couris, C. Fotakis, Appl. Spectrosc. **51**, 1025 (1997)
2 D. Romero, J.M. Fernandez Romero, J.J. Laserna, J. Anal. At. Spectrom. **14**, 199 (1999)
3 Y.Y. Yoon, T.S. Kim, K.S. Chung, K.Y. Lee, G.H. Lee, Analyst **122**, 1223 (1997)
4 G.M. Weyl, Physics of laser-induced breakdown: an update, in *Laser-Induced Plasmas and Applications*, ed. by L.J. Radziemski, D.A. Cremers (Marcel Dekker, New York, 1989)

5 R.E. Russo, Appl. Spectrosc. A **49**, 14 (1995)
6 C. Geertsen, A. Briand, F. Chartier, J.L. Lacour, P. Mauchien, S. Sjöstrom, J.M. Mermet, Anal. At. Spectrom. **9**, 17 (1994)
7 M.A. Shannon, X.L. Mao, A. Fernandez, W.T. Chan, R.E. Russo, Anal. Chem. **67**, 4522 (1995)
8 M. Autin, A. Briand, P. Mauchien, J.M. Mermet, Spectrochim. Acta B **48**, 851 (1993)
9 B.C. Castle, K. Visser, B.W. Smith, J.D. Winefordner, Appl. Spectrosc. **51**, 1017 (1997)
10 E. Tognoni, V. Palleschi, M. Corsi, G. Cristoforetti, Spectrochim. Acta B **57**, 1115 (2002)
11 H.R. Griem, *Plasma Spectroscopy* (McGraw Hill, New York, 1964)
12 T. Fujimoto, R.W.P. McWhirter, Phys. Rev. A **42**, 6588 (1990)
13 M. Capitelli, F. Capitelli, A. Eletskii, Spectrochim. Acta B **55**, 559 (2000)
14 A. De Giacomo, V.A. Shakhatov, O. De Pascale, Spectrochim. Acta B **56**, 753 (2001)
15 G. Colonna, A. Casavola, M. Capitelli, Spectrochim. Acta B **56**, 567 (2001)
16 Y. Iida, Spectrochim. Acta B **45**, 1353 (1990)
17 B. Le Drogoff, J. Margot, M. Chaker, M. Sabsabi, O. Barthélemy, T.W. Johnston, S. Laville, F. Vidal, Y. von Kaenel, Spectrochim. Acta B **56**, 987 (2001)
18 M. Milan, J.J. Laserna, Spectrochim. Acta B **56**, 275 (2001)
19 G. De Giacomo, Spectrochim. Acta B **58**, 71 (2003)
20 D.A. Rusak, B.C. Castle, B.W. Smith, J.D. Winefordner, Spectrochim. Acta B **52**, 1929 (1997)
21 J. Hermann, C. Vivien, A.P. Carricato, C. Boulmer Leborgne, Appl. Surf. Sci. **129**, 645 (1998)
22 A.K. Knight, N.L. Scherbarth, D.A. Cremers, M.J. Ferris, Appl. Spectrosc. **54**, 331 (2000)
23 M. Sabsabi, V. Detalle, M.A. Harith, W. Tawfik, H. Imam, Appl. Opt. **42**, 6094 (2003)
24 D. Bulajic, M. Corsi, G. Cristoforetti, S. Legnaioli, V. Palleschi, A. Salvetti, E. Tognoni, Spectrochim. Acta B **57**, 339 (2002)
25 L.M. Cabalin, J.J. Laserna, Spectrochim. Acta B **53**, 723 (1998)
26 D.A. Cremers, L.J. Radziemski, History and fundamentals of LIBS, in *Laser Induced Breakdown Spectroscopy*, ed. by I. Schechter, V. Palleschi, A.W. Miziolek (Cambridge University Press, Cambridge, 2006)
27 C. Chaleard, P. Mauchien, N. Andre, J. Uebbing, J.L. Lacour, C. Geertsen, J. Anal. At. Spectrom. **12**, 183 (1997)
28 C. Colon, G. Hatem, E. Verdgo, P. Ruiz, J. Campos, J. Appl. Phys. **73**, 4752 (1993)
29 G. Bekefi, C. Deutsch, B. Yaakobi, Spectroscopic diagnostics of laser plasmas, in *Principles of Laser Plasmas*, ed. by G. Bekefi (Wiley Interscience, New York, 1994)
30 J. Bengoechea, C. Aragon, J.A. Aguilera, Spectrochim. Acta B **60**, 904 (2005)
31 H.R. Griem, *Principles of Plasma Spectroscopy* (Cambridge University press, Cambridge, 1997)
32 O. Barthélemy, J. Margot, S. Laville, F. Vidal, M. Chaker, B. Le Drogoff, T.W. Johnston, M. Sabsabi, Appl. Spectrosc. **59**, 529 (2005)
33 E. Tognoni, V. Palleschi, M. Corsi, G. Cristoforetti, N. Omenetto, I. Gornushkin, B.W. Smith, J.D. Winefordner, From sample to signal in laser induced breakdown spectroscopy: a complex route to quantitative analysis, in *Laser Induced Breakdown Spectroscopy*, ed. by I. Schechter, V. Palleschi, A.W. Miziolek (Cambridge University Press, Cambridge, 2006)
34 P.W.J.M. Boumans, Excitation phenomena and temperature measurements, in *Theory of Spectrochemical Excitation*, ed. by P.W.J.M. Boumans (Hilger and Watts, London, 1966)
35 W. Lochte-Holtgreven, Evaluation of plasma parameters, in *Plasma Diagnostics*, ed. by W. Lochte-Holtgreven (Wiley Interscience, New York, 1968)
36 R.W.P. McWhirter, Spectral Intensities, in *Plasma Diagnostic Techniques*, ed. by R.H. Huddlestone, S.L. Leonard (Academic, New York, 1965)
37 A. Casavola, G. Colona, M. Capitelli, Appl. Surf. Sci. **85**, 208 (2003)